PPPL-3310, Preprint: August 1998, UC-420, 426, 427

Fokker-planck Modelling of Delayed Loss of Charged Fusion Products in TFTR

V.A. Yavorskij, J.W. Edenstrasser*, V.Ya. Goloborod'ko, S.N. Reznik, and S. Zweben**

Institute for Nuclear Research, Kiev, Ukraine
*Institute for Theoretical Physics, University of Innsbruck, Austria
**Princeton Plasma Physics Laboratory, New Jersey, United States of America

ABSTRACT

The results of a Fokker-Planck simulation of the ripple induced loss of charged fusion products in TFTR are presented. It is shown that the main features of the measured "delayed loss" of partially thermalized fusion products, such as the differences between DD and DT discharges, the plasma current and major radius dependencies etc., are in satisfactory agreement with the classical collisional ripple transport mechanism. The inclusion of the inward shift of the vacuum flux surfaces turns out to be necessary for an adequate and consistent explanation of the origin of the partially thermalized fusion product loss to the bottom of TFTR.

INTRODUCTION AND REVIEW OF EXPERIMENTAL DATA

The confinement of charged fusion products (FPs) in tokamak-reactors has been the subject of intensive numerical modelling and experimental research during the last years (see for instance Refs. [1-11]). According to the modern understanding of this problem, at least in the MHD-quiescent tokamak plasma, the fast ion behaviour is mainly determined by classical transport processes [2, 3] caused by orbit effects (including those induced by toroidal field ripple) and Coulomb collisions. In spite of the progress in understanding the classical alpha confinement in a tokamak plasma, some of the experimental results -- for example, the origin of a low energy, partially thermalized fusion product loss to the bottom of TFTR -- are not quite

understood [3,5-7]. This kind of loss is also known as "delayed loss", and was observed for DD charged fusion products in the energy range down to about half the birth energy, so was not due to the usual first-orbit loss which occurs only at very near the birth energy.

These delayed loss measurements were made with a scintillator detector located 90 degrees below the outer midplane, as described previously [6, 7]. The main experimental features of the delayed loss were: - (1) its appearance was delayed by 0.2±0.1 *sec* with respect to the normal prompt first-orbit loss, (2) its energy was about 1/2 that of the prompt first-orbit loss, (3) its pitch angle was higher than the first orbit loss, typically 65-70^{o} with respect to the local toroidal field, (4) the relative size of the delayed loss with respect to the first-orbit one increased with plasma current and with NBI power at a fixed current, (5) the delayed loss had a strong dependence on the plasma major radius, appearing strongly at $R < 2.52$ *m* and disappearing at $R > 2.55$ *m*, and (6) the characteristics of this loss process were very reproducible, occurring on every discharge of this type, except for those with strong MHD activity. For DD plasmas with $I = 1.6$ *MA* and $R = 2.45$ *m*, the delayed loss was nearly 4 times larger than the calculated first-orbit loss. The very reproducible nature of this loss suggests that it is not due to MHD activity, which is variable from shot-to-shot. However, the delayed loss can be strongly modulated by such MHD activity, causing it to either increase or decrease. This delayed loss was seen most clearly in the scintillator detector 90^{o} below the outer midplane (in the ion grad-*B* drift direction), and was not seen at other poloidal detector locations, e.g. 60^{o}, 45^{o}, and 20^{o} below the outer midplane.

In DD plasmas, these scintillator detectors measured both 1 *MeV* tritons and 3 *MeV* protons, with a relative response which depends on the energy loss in a 3 micron thick aluminium

foil filter in the detector [5]. The detector response to (half-energy) 1.5 *MeV* protons is about 10 times that of 0.5 *MeV* tritons; therefore it is likely that the delayed loss is dominated by 3 *MeV* protons. However, it is not possible to uniquely identify which species is responsible for the delayed loss, since the detector only measures the gyroradii and not the mass of these lost ions.

In TFTR DT plasmas there was, surprisingly, *no* evidence for any delayed loss of alpha particles as measured by the same scintillator detector 90^{o} below the midplane, i.e. the alpha loss measurements were consistent with simple first-orbit loss [7]. However, an entirely different type of lost alpha detector at the same poloidal location in TFTR *did* show evidence of a partially thermalized alpha loss. The alphas in this detector were collected in a thin metal foil and removed for analysis, so its data was not time-resolved [11]. However, several features of the alpha collector measurements were similar to those of the delayed loss observed for DD fusion products; namely, the ratio between low energy loss and prompt first-orbit loss increased as the plasma current increased (the alpha loss at I=1.0 *MA* was consistent with the first-orbit loss), the peak of the energy of the alpha loss at high current (I=1.8 MA) was about 30% below the birth energy, and the pitch angle of the partially thermalized alpha loss at higher current was larger than the first-orbit loss. At high current, the magnitude of this "delayed" alpha loss in DT was about a factor of 6 above the first-orbit loss for collector samples located 0.5±0.3 *cm* radially inside the limiter radius, but was within a factor of 2 above the first-orbit loss for collector samples located at 0.6±0.3 *cm* radially outside the limiter radius. Since the aperture of the 90^{o} scintillator detector was about 1.2 *cm* outside the limiter radius, it appears as if the delayed alpha loss was strongly shadowed by the limiter in these experiments.

The very reproducible nature of the DD measurements of the delayed loss in the 90^{o} detector suggest that it is due to some classical mechanism. However the simulations of the axisymmetric collisional loss in TFTR [8] are not consistent with the delayed loss measurements [7]. Namely, the pitch-angles of the calculated collisional losses are less than those of the measured first orbit loss and not higher as is measured for delayed loss, and the calculated axisymmetric collisional loss near the bottom of TFTR is significantly smaller than the experimentally observed delayed loss. By employing a Monte Carlo code, in Ref.[9, 10] the collisional loss of the alphas in the presence of TF ripple has previously been simulated for TFTR, where the obtained losses turned out to be significantly larger than the axisymmetric collisional losses [8]. However, in these calculations the losses were peaked poloidally within 30^{o} below the outer midplane [9], a result which is also inconsistent with the delayed loss measurements 90^{o} below the midplane.

The purpose of the present paper is to explain how partially thermalized FPs can reach the detector at the bottom of the vessel, based on a model which includes a significant inward shift of the flux surfaces in the vacuum region [8]. The stochastic ripple diffusion [4] and the superbanana diffusion [13,14] of toroidally trapped fast ions are considered as possible mechanisms which may be responsible for this delayed loss. These investigations are based on the 3D Fokker-Planck code of Ref. [8], which is extended to the case of a rippled tokamak field.

The paper is organised as follows. In Sec. 2 the influence of the inward shift of the flux surfaces in the vacuum region on the poloidal distribution of the loss of partially thermalized alphas is investigated. A qualitative evaluation of the collisional ripple diffusion rate of the

toroidally trapped fast ions is carried out in Sec. 3. The results of a 3D Fokker-Planck simulation of the delayed loss of fusion products in TFTR and comparisons with the experiments are represented in Sec. 4. Finally relevant conclusions are drawn in Sec. 5.

2. MARGINALLY CONFINED ORBITS AND VACUUM FIELD EFFECT

In the present paper we are interested in the ripple loss, caused by the weak perturbation of the axisymmetric particle motion, and neglect the ripple trapping effects. As a mechanism of the charged fusion product loss we consider the radial diffusion induced both by the pitch-angle scattering and the ripple perturbation of particle motion [13-15]. However, here we are not interested in the FP losses due to the pitch angle scattering of counter-circulating particles into the first-orbit loss cone [8, 27, 28]. In this case the losses take place due to the step by step increase of the maximum radius of the orbit. As a result the particle can intersect the wall only near the poloidal angle ϑ_t, corresponding to the tangency point of the marginally confined orbit with the wall. To investigate the tangency condition we first neglect the effects caused by the TF ripples and radial diffusion and employ the model of an axisymmetric magnetic field with shifted circular flux surfaces [8, 16]. Then the major flux surface radius, R_O, is given by

$$R_O(r) = R + \Delta(r)\,, \tag{1}$$

where R is a major plasma radius and $\Delta(r)$ is the shift of the flux surface with minor radius r. It is obvious that the vacuum region (or "gap") between the plasma and the chamber wall can significantly influence the marginally confined orbits (i.e. orbits which become tangent to the wall). In the absence of the gap, the flux surface with the maximum radius coincides with the

chamber wall, so that all slowly outwardly diffusing banana orbits eventually intersect the chamber at poloidal angles close to the midplane. In the presence of a vacuum region between plasma and wall, as in the case of TFTR plasmas with R<2.6 m, the vacuum flux surfaces have to be shifted inwards compared with the plasma surface, in order to satisfy the condition for a currentless gap (i.e. the condition of minimum $\int dS_{vac} j_t^2 [r, \Delta(r), q(r)]$, see [8]). In other words, the major and minor radii of the vacuum flux surfaces are correspondingly smaller and larger than the major and minor radii, R_W and r_W, of the chamber wall. Therefore these surfaces should intersect the chamber wall. As a result the TF ripple diffusion losses for most of the partially thermalized toroidally trapped particles (except deeply trapped ones) can take place far away from the outer midplane [17]. In order to investigate the influence of the vacuum region on the marginally confined orbits, within the plasma the profiles of the flux surface shift $\Delta(r)$ and the safety factor $q(r)$ are determined by TRANSP calculations [8, 18], whereas for the vacuum region the shift is approximated by

$$\Delta(x)/a = \Delta_0 (x^2 - 1) + \Delta_1 (x^2 - 1)^2, \quad q(x) = x^2 q(1), \quad x = r/a, \tag{2}$$

where a is the minor plasma radius and $\Delta_0 = 0.5 \partial\Delta / \partial r|_{r=a}$ is a constant corresponding to results of Refs.[8, 18]. Δ_1 is a constant determining the maximum inward shift Δ_m defined as $\Delta_m = \Delta(r_{max}/a)$, where $r_{max} = R_W + r_W - R - \Delta_m$ is the maximum flux surface radius at $x > 1$. If we assume for Δ_1 the value $\Delta_1 = 0.025$ then the vacuum profiles determined by Eq.(2) allow a very accurate approximation of the currentless profiles obtained in Ref.[8] (see Fig.1). Furthermore, the value of the tangency poloidal angle ϑ_t is then determined by the total and

longitudinal energies of the particles, strongly depending on the maximum inward shift Δ_m. This is confirmed by Fig.2, where the typical marginally confined orbits of 0.5 *MeV* tritons are shown. In fact, in the case of a weak inward shift ($\Delta_m = -0.1a$), a marginally confined orbit is tangent to the chamber wall at the midplane (orbit *B* in Fig.2). However if $\Delta(r)$ and $q(r)$ correspond to the currentless gap, then the tangency angle is situated at $\vartheta_t = 62.5^o$ (orbit *A* in Fig.2, we are interested here only in values ϑ_t below the midplane, where according to the assumed orientation of the ion ∇B drift the loss is possible). In Fig.3 there is represented the dependence of the tangency angle ϑ_t on the value of the maximum inward shift of the vacuum flux surfaces for tritons and alphas at $I = 2MA$ and $R = 2.52\ m$, based on the model profiles of $\Delta(r)$ and $q(r)$ given by Eq.(2). It can be seen that, if Δ_m exceeds some critical value Δ_{cr}, then ϑ_t is shifted poloidally toward the bottom of the TFTR vessel, otherwise $\vartheta_t = 0$. Thus for the 0.5 *MeV* tritons with normalised magnetic moment λ=0.925 it follows from Fig.3 that $\Delta_{cr} = -0.13a$ and that for $\Delta_m = -0.24a$ the tangency angle is situated at $\vartheta = 62^o$, being in agreement with Fig.2.

The poloidal shift of the impact point of the marginally confined orbit tends to result in a poloidal shadowing of the outer midplane region of the toroidally smooth wall from the diffusive loss of FPs. From the expression for the curvature radius, r_{curv}, of the banana orbit at the midplane,

$$r_{curv}(E,\lambda) - r_{\max} \cong -\frac{q(r_{\max})V}{\omega_{B_O}} \frac{1+\xi_m^2}{2\xi_m}, \quad \xi_m = \left(1 - \frac{\lambda R}{R_w + r_w}\right)^{1/2}, \tag{3}$$

it follows that

$$r_{curv}(E,\lambda)\begin{cases} > r_w, & E < E_{cr} \\ < r_w, & E > E_{cr} \end{cases}, \quad r_{curv}(E_{cr},\lambda) = r_w . \tag{4}$$

Here E is the particle energy, $\lambda = (1-\cos^2\chi)B_0 / B$ a transverse adiabatic invariant, χ the particle pitch-angle and B_0 the magnetic field at the plasma centre. Furthermore, ξ_m denotes the particle pitch-angle cosine at midplane, V the particle velocity and E_{cr} the critical energy corresponding to the orbit for which the curvature radius at the midplane is identical to the minor wall radius. Note that this E_{cr} corresponds to a critical gyroradius ρ_{cr} which may be approximated by $\rho_{cr} \approx 2(R_w - R - \Delta_m)\xi_m / q(r_{\max})$. Since the curvature radius r_{curv} decreases with increasing *E,* the tangency requirement may be written as $r_M(\vartheta_t, E, \lambda) = r_w$, where r_M is the maximum distance from the chamber centre and $\vartheta_t = 0$ for $E > E_{cr}$ and $\vartheta_t \neq 0$ for $E < E_{cr}$. From the expansion of this tangency condition in the vicinity of $\vartheta_t = 0$ and $E = E_{cr}$ then it follows

$$\sin\frac{\vartheta_t}{2} \propto \begin{cases} \left(1 - \frac{E}{E_{cr}}\right)^{1/2}, & E \le E_{cr} \\ 0, & E > E_{cr} \end{cases} . \tag{5}$$

From Fig. 3 it is concluded that the analytical approximations of Eqs. (3-5) are in agreement with the numerical results, also showing the strong dependence of ϑ_t on the particle energy. Thus relatively few particles can be lost at $\vartheta < \vartheta_t$ as a result of radial diffusion if there is only a small change of the energy and radial position of the banana tip per bounce. This effect becomes stronger with decreasing both major plasma radius and particle energy (see Figs.4, 3) and, obviously, with increasing plasma current, as all of them result in a banana width reduction and in the enhancement the influence of vacuum field. In the following we will refer to this as the

poloidal shadowing effect, in contrast to the toroidal shadowing effect due to the toroidally non-smooth nature of the limiters in TFTR [19].

In order to take into account the influence of the magnetic field ripples on the marginally confined particles, the TFTR magnetic field is approximated by the expression $\mathbf{B} = \mathbf{B}^{s} + \mathbf{B}^{r}$, where $\mathbf{B}^{s}$ is the model magnetic field of an axisymmetric toroidal configuration with nested-in circular flux surfaces [8, 16] and $\mathbf{B}^{r} = \nabla U$ is the ripple perturbation. The perturbation potential U can be expressed in the form $U = (F\delta / N)\sin N\varphi$, where F is the poloidal current outside the considered flux surface, N is the number of TF coils, and δ is the ripple amplitude, which is modelled by [20]

$$\delta = \delta_0 I_0(N\eta), \quad \eta^2 = \frac{(R_r - r)^2 + z^2}{R_r r}, \tag{6}$$

with $I_0(x)$ being the modified Bessel function. Furthermore, in accordance with Ref.[21] it is assumed $N = 20$, $R_r = 2.25m$ and $\delta_0 = 1.4 \cdot 10^{-5}$.

Because of the uncompensated vertical ripple drift of trapped particles at the bounce point, the poloidal and pitch angles of the lost fusion products can be significantly increased [22]. This effect is demonstrated in Fig.5, where both, the ripple perturbed as well as the unperturbed orbits of the alphas are represented. To obtain a qualitative description of the influence of the ripples on the angular distribution of lost particles, it is assumed that the lost bananas are homogeneously distributed over all the values of the vertical ripple drift d per bounce period in the range

$$d_m \le d \le 0, \tag{7}$$

where d_m is the amplitude value of this drift per bounce [4, 15], defined by

$$d_m = \frac{q\rho_L(\delta/2)^{1/2}}{\varepsilon}\begin{cases} (2\pi/\alpha)^{1/2}, & \alpha > 1 \\ \alpha\ln(16e)/(\pi\alpha), & \alpha < 1 \end{cases}, \tag{8}$$

with $\alpha \cong |z|/(NqR_o\delta)$ and $\varepsilon = r/R_o$. Note, that the maximum ripple drift per bounce period $d = 2d_m$ only applies to those particles, which strictly satisfy the resonance condition (see Sec.3). However, since the fraction of the latter is only small as compared with the total number of the diffusively lost particles, one can neglect their contribution to the poloidal and pitch-angle distributions.

The ripple induced change in the poloidal angle at which the orbit hits the wall, $\Delta\vartheta = \vartheta - \vartheta_t$, strongly depends on ϑ_t. It follows from the analytical analysis (similar to that of Ref. [22]) of the ripple perturbed banana motion that for small ϑ_t this change is of the order $(\varepsilon d/\Delta r_b)^{1/4}$, and near the vessel bottom $\Delta\vartheta \propto (\varepsilon d/\Delta r_b)^{1/2}$, where Δr_b is the characteristic banana width. The typical increase of the poloidal angle for lost FPs given by these approximate expressions, $\Delta\vartheta \le 10^o \div 30^o$, is in agreement with the modelling results shown in Fig. 5.

3. SUPERBANANA DIFFUSION

The orbits of toroidally trapped fast particles in tokamaks are known to be very sensitive to weak field-asymmetries caused by TF ripples. Therefore, most sensitive to ripple perturbations are the so called resonant particles [15, 23], satisfying

$$l\omega_b = N\omega_d, \quad l = 0,\pm1,\pm2,... \tag{9}$$

where ω_b and ω_d are the particle bounce and precession frequencies, respectively. Fig.6 represents typical resonant levels for 3.5 *MeV* alphas in the $\{\lambda, r_m\}$ plane, where r_m is the maximum radial coordinate along the unperturbed orbit. In this section, we will consider the toroidally trapped particles within the non-stochastic domain, which are confined in the absence of collisions. In the vicinity of the resonant levels, these particles execute "superbanana" orbits [14, 15, 17] with typical radial excursions in the order of

$$\Delta r_{sb} \le r_m / \Delta l_r, \tag{10}$$

where Δl_r is the number of resonant levels in the radial coordinate within the non-stochastic domain. It should be pointed out that the superbanana radial excursions are significantly larger than the typical ripple induced drift *d* of the banana tip per bounce. Typical values of *d* in TFTR are about 1 *cm* [20], while Δr_{sb} is of the order 5-10 *cm*. This is demonstrated in Fig.7 by the time dependence of r_m for alphas with $\lambda = 0.9$, obtained by numerical integration of the equations of motion. Typical periods of superbanana oscillations are in the order of 10-20 banana bounce times.

In the presence of weak pitch-angle scattering, superbanana excursions result in a collisional ripple diffusion with a rate

$$D^r = \nu_{eff}\left(\Delta r_{sb}\right)^2, \quad \nu_{eff} = \nu_\perp \varepsilon / \left(\Delta\lambda_{sb}\right)^2, \tag{11}$$

where ν_{eff} is the effective pitch-angle scattering rate of superbananas in the λ variable and ε is the inverse aspect ratio. The width $\Delta\lambda_{sb}$ of a resonant region satisfies the relation

$$\Delta\lambda_{sb} \le \varepsilon / \Delta l_{\lambda}, \tag{12}$$

where Δl_{λ} is the number of resonant levels for a fixed r_m. With the help of Eqs. (9) and (10), the collisional ripple diffusion coefficient D^r can be estimated by the relation

$$D^r = D_{sb}\left(\Delta l_{\lambda} / \Delta l_r\right)^2, \quad D_{sb} = \nu_{\perp} r_m^2 / \varepsilon. \tag{13}$$

Note that the diffusion coefficient D_{sb} looks like the standard "superbanana" diffusion [12,24], and the factor $\left(\Delta l_{\lambda} / \Delta l_r\right)^2$ accounts for the effect of "inclination" of resonant levels in the $\{\lambda, r_m\}$ plane. The maximum diffusion takes place if resonant levels are parallel to line $\lambda = const$.

It should be pointed out that D_{sb} can be derived also from qualitative expressions for the superbanana motion of alphas in the limit of a small banana width [15]. If we employ for Δr_{sb}, ν_{eff} and the frequency of superbanana oscillations ν_{sb} the formulas derived in Refs. [15, 25], then one arrives at the relations

$$\Delta r_{sb} \cong \frac{r}{Nq}\left(1+\sqrt{\frac{\delta_1}{\delta}}\right)^{-1}, \quad \nu_{eff} \cong \frac{\nu_{\perp} N^2 q^2}{\varepsilon}\left(1+\sqrt{\frac{\delta_1}{\delta}}\right)^2, \quad \nu_{sb} \cong \frac{V_d}{r}\left(\frac{\delta}{\delta_1}+\sqrt{\frac{\delta}{\delta_1}}\right). \tag{14}$$

Here $\delta_1 = \varepsilon / (Nq)^{3/2}$ is the characteristic ripple value that divides the plasma into regions with qualitatively different superbanana motions [15, 23-25] and V_d is the toroidal drift velocity. It may be easily seen that Δr_{sb} and ν_{eff}, defined by Eqs.(14) also result in the diffusion coefficient $D^r \cong D_{sb}$. This rate corresponds to the regime of weak collisionality with $\nu_{eff} < \nu_{sb}$ and applies for particles with high energies, which satisfy the inequality

$$\left(\frac{E}{E_0}\right)^{5/2} > \frac{\nu_\perp(E_0)R}{V_d(E_0)} N^2 q^2 \frac{\delta_1}{\delta}\left(1+\sqrt{\frac{\delta_1}{\delta}}\right), \tag{15}$$

where E_O is the birth energy of the charged fusion product. For typical TFTR parameters the condition for weak collisionality is satisfied for $E / E_0 \geq (0.3 \div 0.5)$. It is evident that the collisional diffusion coefficient D^r can be comparable to the one of the superbananas D_{sb} only in resonant regions, i.e., in the vicinity of resonant levels, where superbanana orbits may occur, whereas outside these regions the inequality $D^r << D_{sb}$ holds. According to the numerical results shown in Fig.7, the volume of the resonant regions is comparable or less than the volume of the non-resonant ones. To examine the effect of a decrease of the ripple diffusion rate due to the existence of non-resonant regions, D^r may be approximated by

$$D^r \cong kD_{sb}, \quad k \leq 1. \tag{16}$$

The evaluation of k is a rather complex theoretical problem and is beyond the scope of the present paper [24]. In our numerical modelling we will apply $k = const$. It should be pointed out that the diffusion coefficient of Eq.(16) is in qualitative agreement with the results of numerical modelling of collisional ripple diffusion of trapped alphas within the central region of a tokamak plasma [26].

4. SIMULATION RESULTS AND COMPARISON WITH EXPERIMENT

The superbanana diffusion should result in an enhanced loss of the toroidally trapped FPs. To evaluate this loss, we carry out the modelling based on the numerical solution of the 3D Fokker-Planck equation in the COM space [8]

$$\nabla_{\mathbf{c}}\left(\mathbf{d}-\ddot{\mathbf{D}}\nabla_{\mathbf{c}}\right)f = S(\mathbf{c}), \tag{17}$$

with $\mathbf{d}=\mathbf{d}^{\mathbf{s}}$, $\ddot{\mathbf{D}}=\ddot{\mathbf{D}}^{\mathbf{s}}+\ddot{\mathbf{D}}^{\mathbf{r}}$ and where the superscripts "*s*" and "*r*" denote the axisymmetric and ripple induced transport coefficients, respectively, $S(\mathbf{c})$ is a source term and $\mathbf{c}$ are the COM variables. The definition domain of the toroidally trapped particles for the case, where the ripple transport is taken into account, is shown in Fig.6. For the calculation of the radial component of $\ddot{\mathbf{D}}^{\mathbf{r}}$, the stochastic diffusion coefficient [4] $D^r = \Delta^2 / (2\tau_b)$ is employed for the stochasticity part of this domain, whereas the superbanana rate of Eq.(12), $D^r = k\nu_{\perp} rR = (10^2\text{-}10^3)\ cm^2/s$ is used for the remainder. The FP loss level will be characterised by that fraction of particles lost for a given species within a given energy range ($E_O > E > mV^2/2$) and poloidal angle.

We first estimate the contribution of the superbanana diffusion to the total diffusive loss of charged fusion products. For a 2 *MA* TFTR discharge with R=2.52 *m*, the dependence of the relative FP loss fraction on the particle velocity for different rates of the assumed ripple induced collisional diffusion is shown in Fig.8. It can be seen that about 5% of the tritons are lost in the high energy range (E/E_O > 0.8), where the main loss mechanism is the ripple induced stochastic diffusion. For k>0.1, the loss fraction of the partially thermalized particles with energies in the range of $0.5<E/E_O<0.8$ is larger than of those with energies in the range $E/E_O>0.8$. The loss of partially thermalized ions scales approximately like $k^{0.5}$. It is similar to the Z_{eff} dependence of the loss due to pitch angle scattering through the trapped-passing boundary [27, 28]. The fraction of the collisional ripple loss of alphas at k = 0.1 is about 7% and comparable to the ripple loss

energy fraction of alpha particles simulated by Monte Carlo code ORBIT [9]. In the following our modelling will be done mainly for an assumed $k = 0.1$.

Note that at $I = 2$ *MA* and $D^r = 0.1\,\nu_\perp\, rR$ the calculated collisional ripple loss of toroidally trapped tritons with $0.5<E/E_O<0.8$ even exceeds the first-orbit loss. In the case of the alphas it is only about 20% of the total loss level. It should be pointed out, that because of the scattering through the passing/trapped boundary it is possible also for originally circulating fusion products to be lost due to the transport mechanism considered. However the quantitative evaluation of the contribution of the circulating at birth particles to the ripple collisional loss was not investigated here.

Now we investigate, for the different detectors in the DT and DD discharges with 2 *MA* and 2.5 *MA* plasma currents, the dependence of the calculated FP loss fraction on energy. First of all it is evident that one has to expect different loss spectra at small and large poloidal angles. Indeed it follows from Sec. 2 that the effect of poloidal shadowing of the outer part of the first wall is extremely sensitive to the energy of the lost particles. Thus, poloidal shadowing takes place only for energies below some critical value E_{cr}. Furthermore, for energies E close to the E_{cr} the tangency angle ϑ_t is strongly increasing with decreasing energy. Therefore, diffusive losses of particles with energies $E> E_{cr}$ should be expected just below the midplane, while the particles with energies $E< E_{cr}$ (except the small number of those with E very close to E_{cr}) should be lost far from the midplane. Hence if the critical energy E_{cr} is close to the birth energy E_O (like in the case of $R = 2.52$ *m* and $I = 2$-2.5 *MA*), then the loss of high energy FPs is expected at small poloidal angles. This is in qualitative agreement with the modelling results represented in Fig.9. Thus for

poloidal angles $\theta < 60°$, the main contribution to the calculated loss comes from the high-energy range $0.8 < E/E_O < 1$ (due to stochastic diffusion) whereas the contribution of the partially thermalized particles is weak. From Fig. 9b it can be concluded that at small poloidal angles the diffusive loss of tritons with $0.5 < E/E_O < 0.8$ is at least a few times smaller as compared with the high-energy loss (including first-orbit one). In the case of the alphas (Fig.9a) this distinction increases. On the other hand at the 90^o detector the energy spectrum of the diffusive loss of FPs is quite different from that at the other detectors. Thus at $\theta = 90^o$ only the collisional loss of particles with E/E_O<0.7-0.8 is observed. Moreover for $I = 2.5$ *MA* the loss of the partially thermalized tritons exceeds the first orbit one. As already pointed out the reason for this difference is the poloidal shadowing of the 20^o, 45^o and 60^o detectors from the collisional loss of thermalized FPs discussed in Sec.2. Note that the weak loss of FPs with energies $0.5<E/E_O<0.8$ at $\theta < 60^o$ is in qualitative agreement with the delayed loss observations (see Sec.1). It can also be seen that the ripple loss at the 20^o and 45^o detectors increases with the plasma current, while at 60^o it decreases. This feature indicates the strong dependence of the poloidal distribution of the ripple loss on the q profile and may be important for the explanation of the inconsistency between the alpha ripple loss measured by the 20^o movable scintillator detector and the total TF ripple loss simulated with ORBIT code [18].

The calculated collisional ripple losses of DD tritons and DT alphas at the 90^o detector are shown in Fig.10. In the energy range $E/E_O > 0.5$ the partially thermalized triton loss significantly exceeds that for the alphas, qualitatively consistent with the delayed loss

measurements [3,5-7]. The differences between the DD and DT FP losses are due to their different collision rates, since for the alphas the ratio of pitch-angle scattering frequency to the slowing down one is about 7 times smaller as in the case of the tritons [7]. As for the case of DD protons this ratio is only 10% that of tritons, the proton contribution to the collisional loss fraction of DD FPs is small as compared with the triton one. More quantitative comparisons with the measurements are difficult since the detector does not distinguish between the proton and triton fusion products [5], moreover the modelling carried out is rather qualitative one and neglect the toroidal shadowing caused by RF limiter (i.e. the radial dependence of alpha loss), the finite Larmor radius effects and so on.

The next important feature of the calculated collisional losses to the 90° detector is the strong dependence of the ratio between delayed loss and first-orbit loss on the plasma current. In fact, from Fig.10a it follows that for energies $E/E_O > 0.5$ the fraction of delayed alpha loss for $I = 2$ *MA* is negligible compared to the 2.5 *MA* case. For tritons the delayed loss fraction for $I = 2.5$ *MA* is about 5 times larger compared to the case $I = 2$ *MA*. This feature of the calculated loss of partially thermalized FPs is also in agreement with experimental observations of the DD FP loss [7].

In Fig.5 of Sec.2 it was shown that the poloidal distribution of lost FPs is strongly affected by the ripple induced drift of banana tips. In Fig. 10a by the curve *a* the significant weakening of the alpha loss for $E/E_O > 0.5$ at the 90° detector is shown for the case where the amplitude value of this drift is assumed to be _ of that given by Eq. (8), i.e. for the range of the vertical ripple drift given by $0.5d_m \le d \le 0$.

Finally curve *b* in Fig. 10b demonstrates the weak increase of the triton loss as a result of the two fold decrease of the threshold for the stochastic ripple diffusion. From the results of the modelling represented in Fig.10b it follows also that the triton loss fraction detected at the 90° detector roughly scales with *k* like $k^{0.5}$, in agreement with the analogous scaling for the calculated total loss of tritons (see Fig. 8).

The pitch-angle distributions of the collisional ripple loss of tritons and alphas at the 90° detector are shown in Fig.11. It can be seen that for $E/E_O > 0.5$ the maximum loss occurs in the pitch-angle range 65°-75°, also being in approximate agreement with the observations [7].

Note that the ripple collisional loss caused by radial diffusion with $D \propto \nu_{\perp} rR$ should increase with NBI power. Really the increasing of the latter results in the increase of the plasma temperature, and hence the decrease of the ratio of pitch angle scattering time to the slowing down one. From the other hand, the NBI induced additional shift of plasma flux surfaces should enhance the inward shift of vacuum ones, and hence should result in the additional shift of delayed loss to the vessel bottom.

5. SUMMARY

A Fokker-Planck simulation of the delayed loss experiments of charged fusion products in TFTR shows that the main observed features are at least qualitatively consistent with the classical collisional ripple transport mechanism. The new feature of these calculations is the

inclusion of an improved model for the vacuum magnetic fields, which can strongly affect the poloidal distribution of the charged fusion ripple loss to the wall.

It is found that the superbanana and stochastic diffusion of toroidally trapped particles in TFTR results in a loss of partially thermalized DD FPs ($0.5<E/E_O<1$) which exceeds the first-orbit loss at $I > 2$ *MA*. In the case of DT plasma with $I = 2$ -2.5 *MA* the calculated loss of partially thermalized alphas is less then the first-orbit one.

The poloidal and pitch angle distributions of the calculated losses have turned out to be very sensitive to the spatial distribution of the magnetic field in the vacuum region. The origin of the losses to the bottom of TFTR in the small pitch-angle range above the passing/trapped boundary may be explained by the effect of poloidal shadowing of the outer part of vessel wall because of the inward shift of the vacuum flux surfaces. For currents $I = 2$-2.5 *MA* the calculated delayed losses at the 90^o detector are characterised by pitch-angles in the range 60^o-75^o and gyroradii < 3.7 - 4.5 *cm* for tritons and < 3.3 - 4 *cm* for alphas, correspondingly. Moreover in the energy range $0.5 < E/E_O < 1$ the calculated triton losses are a few times larger than those for alphas, which helps to explain the absence of any significant delayed loss of alphas in DT.

It is found that at poloidal angles $\leq 60^o$ the collisional ripple loss of partially thermalized DD and DT fusion products is small as compared with the loss of high-energy ones. This is consistent with the apparent absence of delayed loss in the DD measurements at these angles. Furthermore, the dependencies of the calculated collisional ripple losses of the charged fusion products on the plasma current and the major plasma radius are shown to be in qualitative agreement with the delayed loss measurements [7].

In summary, the collisional ripple loss mechanism is at least qualitatively consistent with previous observations of the delayed loss of DD fusion products in TFTR. This loss mechanism may also explain the anomalous loss of partially thermalized alphas measured by the TFTR alpha collector [11]. However, for quantitative comparisons of the calculated and measured loss levels these simulations should be carried out with more accurate transport coefficients, and should also take into account the toroidal shadowing caused by RF limiter (i.e. the radial dependence of alpha loss) and the finite Larmor radius effects, which were neglected in our consideration. This collisional ripple loss mechanism should play an important role in the alpha particle loss behaviour in the large scale tokamaks like ITER, since the role of ripple collisional loss mechanism of FPs dominates over the first-orbit loss at high plasma current, and the issue of the spatial distribution of the alpha loss to the first-wall is crucial to the design of the first-wall structure and TF magnet systems.

Acknowledgements

This work was supported, in part, by the Austrian ÖAW-Euratom-Association, Project P8 and Grants # 2.5.2/8 and 2.4/176 of the Ministry of Science and Technologies of Ukraine. This work was also partially supported by PPPL under subcontract S-04076-F.

Figure Captions

Fig. 1 Profiles of Shafranov shift (figure (*a*)) and safety factor (figure (*b*)) used for the investigation of the marginally confined orbits. Curves *A* correspond to the model of a currentless gap [7], curves *B* and *C* are given by Eq. (2) with $\Delta_1 = 0.1$ and $\Delta_1 = 0.02$, respectively. **r-R** is the distance in the equatorial plane from the plasma centre.

Fig. 2 Marginally confined orbits of tritons with λ=0.925 ($\lambda = (1 - \cos^2 \chi) B_0 / B$ is a transverse adiabatic invariant, χ is the particle pitch-angle and B_0 the magnetic field at the plasma centre). Orbits *A* and *B* correspond to the *A* and *B* vacuum profiles of shift and safety factor in Fig. 1. ϑ_t is the poloidal angle corresponding to the tangency point. $\vartheta_t = 62.5^o$ for the orbit *A* and $\vartheta_t = 0^o$ for the orbit *B*. **r-R** is the distance in the equatorial plane from the plasma centre.

Fig. 3 Tangency poloidal angle versus maximum inward shift of the vacuum flux surfaces for the model profiles of $\Delta(r)$ and $q(r)$ given by Eq. (2).

Fig. 4 Marginally confined orbits of tritons with λ=0.925 for a major plasma radius R = 2.45 *m*. Tangency poloidal angles ϑ_t are 90.2° and 74.6° for particle energies 0.5 *MeV* and 1 *MeV,* respectively. **r-R** is the distance in the equatorial plane from the plasma centre.

Fig. 5 Marginally confined orbits of tritons with λ=0.925 in the presence of TF ripple. θ and χ are the poloidal and pitch angles at the impact point. Orbits 1, 2 and 3 in figure (*a*) start at toroidal angles at the tangency point above the midplane, φ = 29.2°, 28.9° and 28.8°,

respectively. In figure *b* these toroidal angles are correspondingly 28° and 11.9° for orbits 1 and 2. Orbits 3 (figure *a*) and 2 (figure *b*) are practically unperturbed by TF ripple. **r-R** is the distance in the equatorial plane from the plasma centre.

Fig. 6 Definition domains of toroidally trapped alphas in the $\{\lambda\ ,\ r_{\mathrm{m}}\}$ plane. *l* is the resonance number (see Eq. (9)). Curves *A* correspond to ripple magnitude $\delta = \delta_1$, where $\delta_1 = \varepsilon/(Nq)^{3/2}$ is the characteristic ripple value which divides the plasma into regions with qualitatively different superbanana motions. Curves B and C correspond to the boundary of stochastic part of definition domain in the case of $\delta_{st} = \delta_{GWB}$ and $\delta_{st} = 0.5\delta_{GWB}$, respectively. Here $\delta_{GWB} = [\varepsilon/(Nq\delta)]^{3/2}(1/\rho_L q')$ is the Goldston, White, Boozer threshold for stochastic ripple loss.

Fig. 7 Time dependence of the maximum radial coordinate on the banana orbit, r_m, for alphas with $\lambda = 0.9$. $\mathrm{T_{norm}}$ is the typical bounce time.

Fig. 8 FP loss fraction in the 2 *MA* TFTR discharge with $R = 2.52$ *m* versus the particle velocity for different rates ($k = 0.1, 0.3, 0.6$) of the ripple collisional diffusion, $D^r = k\nu_\perp rR$.

Fig. 9 FP loss fractions versus the particle velocity at the poloidal angles 20, 45, 60 and 90 degrees. Loss curves are normalised to the first orbit loss $L_{90}^{FO}(I)$ at $\theta = 90^{\circ}$. $L_{90}^{FO}(2MA) \cong 2\,L_{90}^{FO}(2.5MA)$; ($L_{90}^{FO}(I)$ for tritons)/($L_{90}^{FO}(I)$ for alphas)$\cong 0.8$.

Fig. 10 Charged fusion product loss fractions at $\theta = 90^{\circ}$. Curve *a* of figure (*a*) corresponds to the two-fold reduced ripple drift of the banana tips. Curve *b* of figure (*b*) is obtained for

$\delta_{st} = 0.5\delta_{GWB}$ i.e. for the two-fold decreased threshold for the stochastic ripple diffusion as compared with the rest curves. Loss curves are normalised to the first orbit loss at θ = 90º. $L_{90}^{FO}(2MA) \cong 2\,L_{90}^{FO}(2.5MA)$; ($L_{90}^{FO}(I)$ for tritons)/($L_{90}^{FO}(I)$ for alphas)$\cong 0.8$.

Fig. 11 Pitch angle distributions of the loss of partially thermalized FPs at the 90º detector.

References

[1] FURTH, H.P., GOLDSTON, R.J., ZWEBEN, S.J.,SIGMAR, D.J., Nucl. Fusion **30** (1990) 1799.

[2] SIGMAR, D.J., CHENG, C.Z., SADLER, G.J., ZWEBEN, S.J., Nucl. Fusion **35** (1995) 1421.

[3] ZWEBEN, S.J., et al, Plasma Phys. Control. Fusion **39** (1997) A275.

[4] GOLDSTON, R.J., WHITE, R.B., BOOZER, A.H., Phys. Rev. Lett. **72** (1974) 2895.

[5] ZWEBEN, S.J., et al, Nucl. Fusion **31** (1991) 2219.

[6] ZWEBEN, S.J., et al, Phys. Plasmas **1**(5) (1994) 1469.

[7] ZWEBEN, S.J., et al, Nucl. Fusion **35** (1995) 893.

[8] GOLOBOROD'KO, V.Ya., REZNIK, S.N., YAVORSKIJ, V.A., ZWEBEN, S.J., Nucl.Fusion **35** (1995) 1523.

[9] REDI, M.H., et al, Nucl. Fusion **35** (1995) 1191.

[10] REDI, M.H., et al, Nucl. Fusion **35** (1995) 1509.

[11] HERRMANN, H.W., et al., Nucl. Fusion, **37** (1997) 293.

[12] GALEEV, A.A., SAGDEEV, R.Z., in Problems of Plasma Theory **7** (1973) 257.

[13] BOOZER, A.H., Phys. Fluids **26** (1980) 2283.

[14] YUSHMANOV, P.N., Review of Plasma Physics, Ed. B.B.Kadomtev, Vol. **16**, Consultant Bureau, New York - London, 1987.

[15] BELIKOV, V.S., KOLESNICHENKO, Ya.I., YAVORSKIJ, V.A., Fusion Technology **15** (1989) 1365.

[16] YAVORSKIJ, V.A., Ukr. Phys. J., **41** (1996) 160.

[17] YAVORSKIJ, V.A., EDENSTRASSER, J.W., GOLOBOROD'KO, V.Ya., REZNIK, S.N., ZWEBEN, S.J., in Alpha Particles in Fusion Research (Proc. IAEA TCM 1997), JET Joint Undertaking, Abingdon (1997) 29.

[18] BUDNY, R.V., ET AL., Nucl. Fusion **34** (1994) 1247.

[19] ZWEBEN, S.J., et al, "Effects of q(r) on the Alpha Particle Ripple Loss in TFTR", (to be published in Nuclear Fusion).

[20] GOLOBOROD'KO, V.Ya., KOLESNICHENKO, Ya.I., YAVORSKIJ, V.A., in Plasma Physics and Controlled Nuclear Fusion Research 1984 (Proc. 10th Int. Conf. London, 1984), Vol. 2, IAEA, Vienna (1985) 179.

[21] BOIVIN, R.L., WHITE, R.B., ZWEBEN, S.J., Nucl. Fusion **33** (1993) 449.

[22] GOLOBOROD'KO, V.Ya., YAVORSKIJ, V.A., Nucl. Fusion **29** (1989) 1025.

[23] GOLOBOROD'KO, V.Ya., KOLESNICHENKO, Ya.I., YAVORSKIJ, V.A., Physica Scripta **T16** (1987) 46.

[24] YAVORSKIJ, V.A., EDENSTRASSER, J.W., GOLOBOROD'KO, V.Ya., ANDRUSHCHENKO, Zh.N., "3D Fokker-Planck equation for fast ions in a tokamak with weak TF ripples" (in preparation).

[25] GOLOBOROD'KO, V.Ya., LUTSENKO, V.V., REZNIK, S.N., KOLESNICHENKO, Ya.I., YAVORSKIJ, V.A., Fusion Technology **18** (1990) 429.

[26] BITTONI, E., HAEGI, M., Fusion Technology **18** (1990) 373.

[27] CHANG, C.S., et al., Phys. Plasmas **1** (1994) 3857.

[28] GOLOBOROD'KO, V.Ya., LUTSENKO, V.V., REZNIK, S.N., YAVORSKIJ, V.A., Fusion Technology **27** (1995) 277.

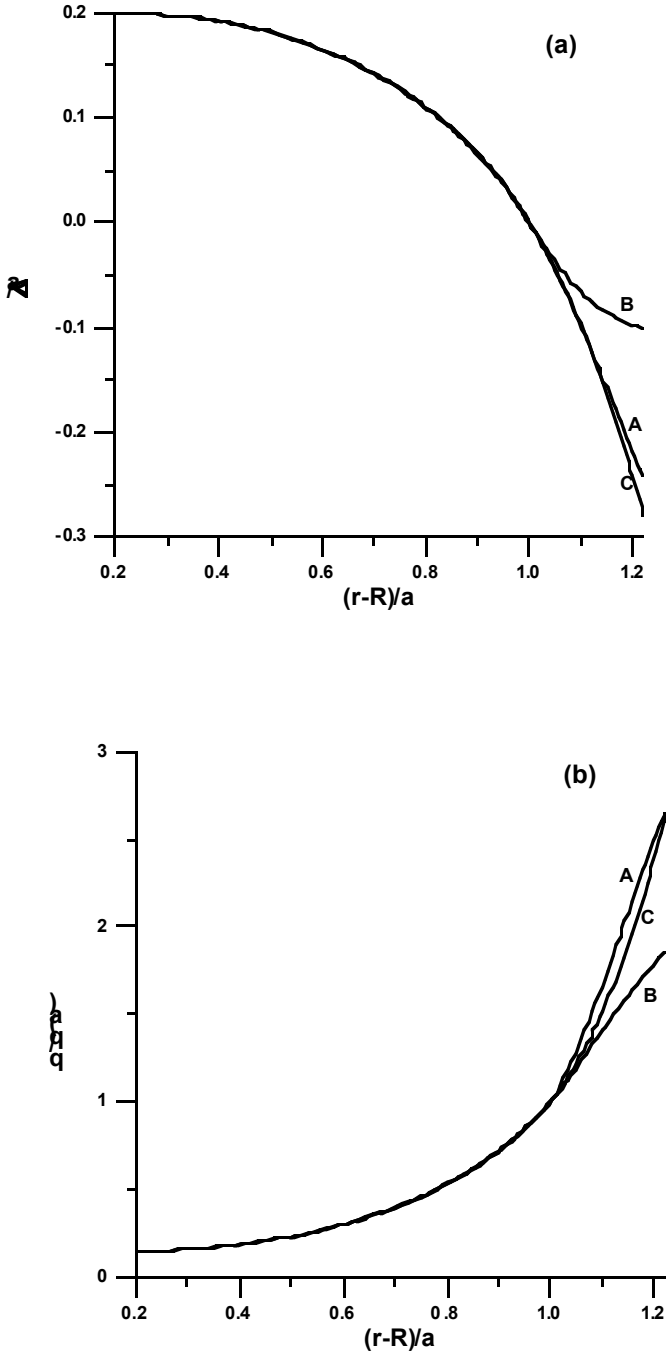
(a)
0.2
0.1
0.0
-0.1
-0.2
-0.3
0.2
0.4
0.6
0.8
1.0
1.2
(r-R)/a
B
A
C
(b)
3
2
1
0
0.2
0.4
0.6
0.8
1.0
1.2
(r-R)/a
A
C
B

Fig. 1

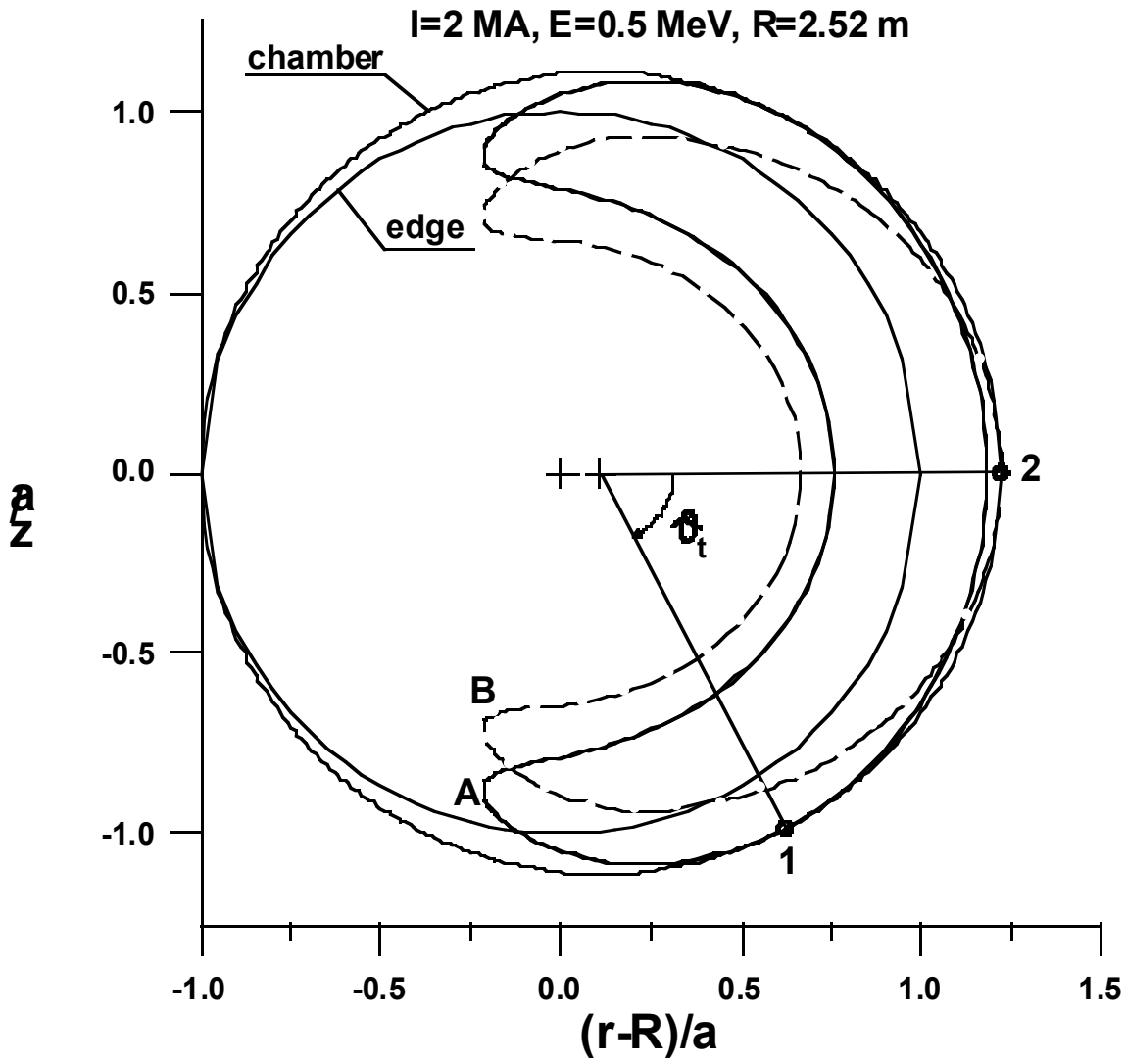
I=2 MA, E=0.5 MeV, R=2.52 m
chamber
edge
1.0
0.5
0.0
-0.5
-1.0
z/a
B
A
1
2
θt
-1.0
-0.5
0.0
0.5
1.0
1.5
(r-R)/a

Fig. 2

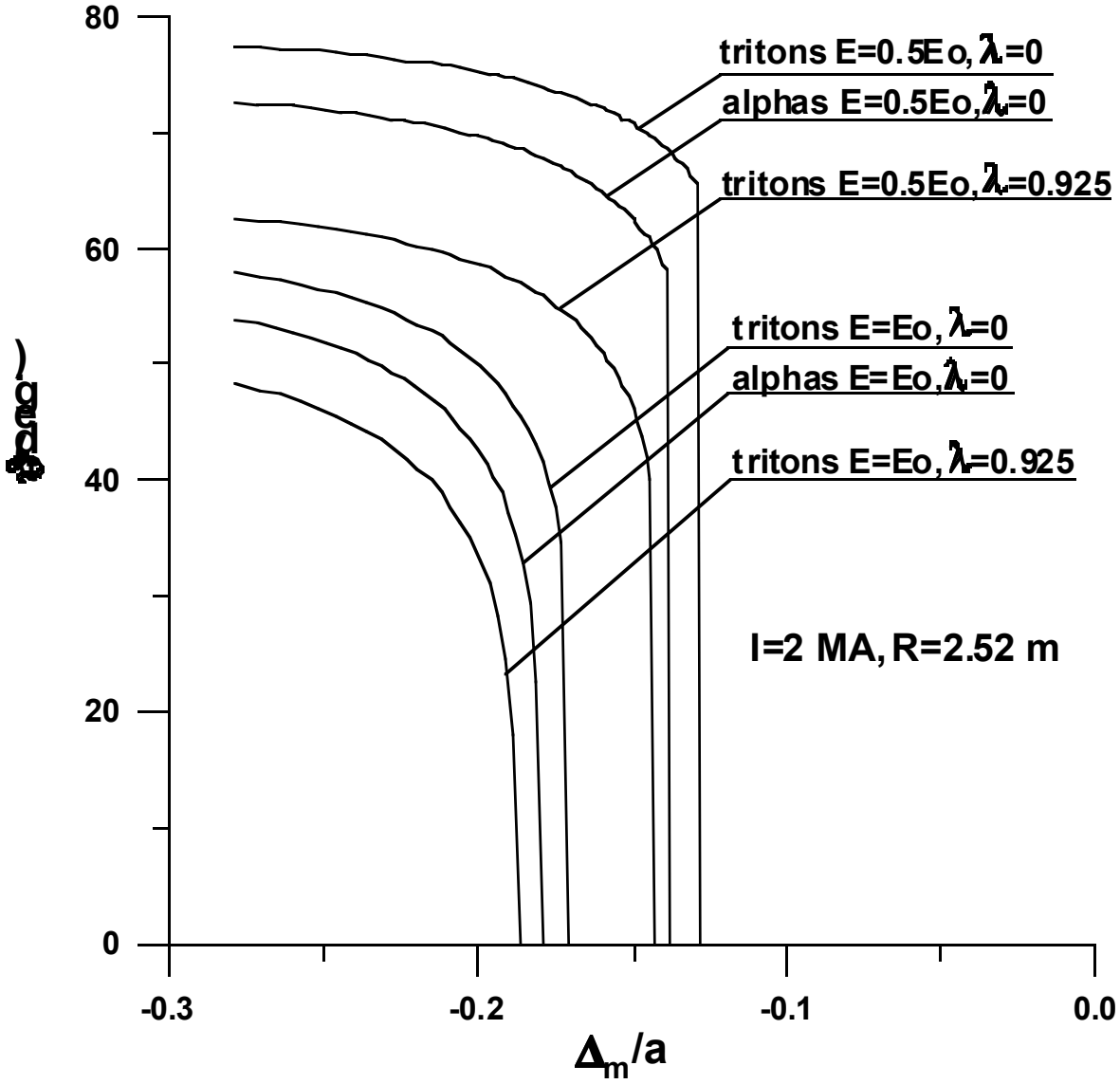
80
60
40
20
0
-0.3
-0.2
-0.1
0.0
Δ_m/a
tritons E=0.5Eo, λ=0
alphas E=0.5Eo, λ=0
tritons E=0.5Eo, λ=0.925
tritons E=Eo, λ=0
alphas E=Eo, λ=0
tritons E=Eo, λ=0.925
I=2 MA, R=2.52 m

Fig. 3

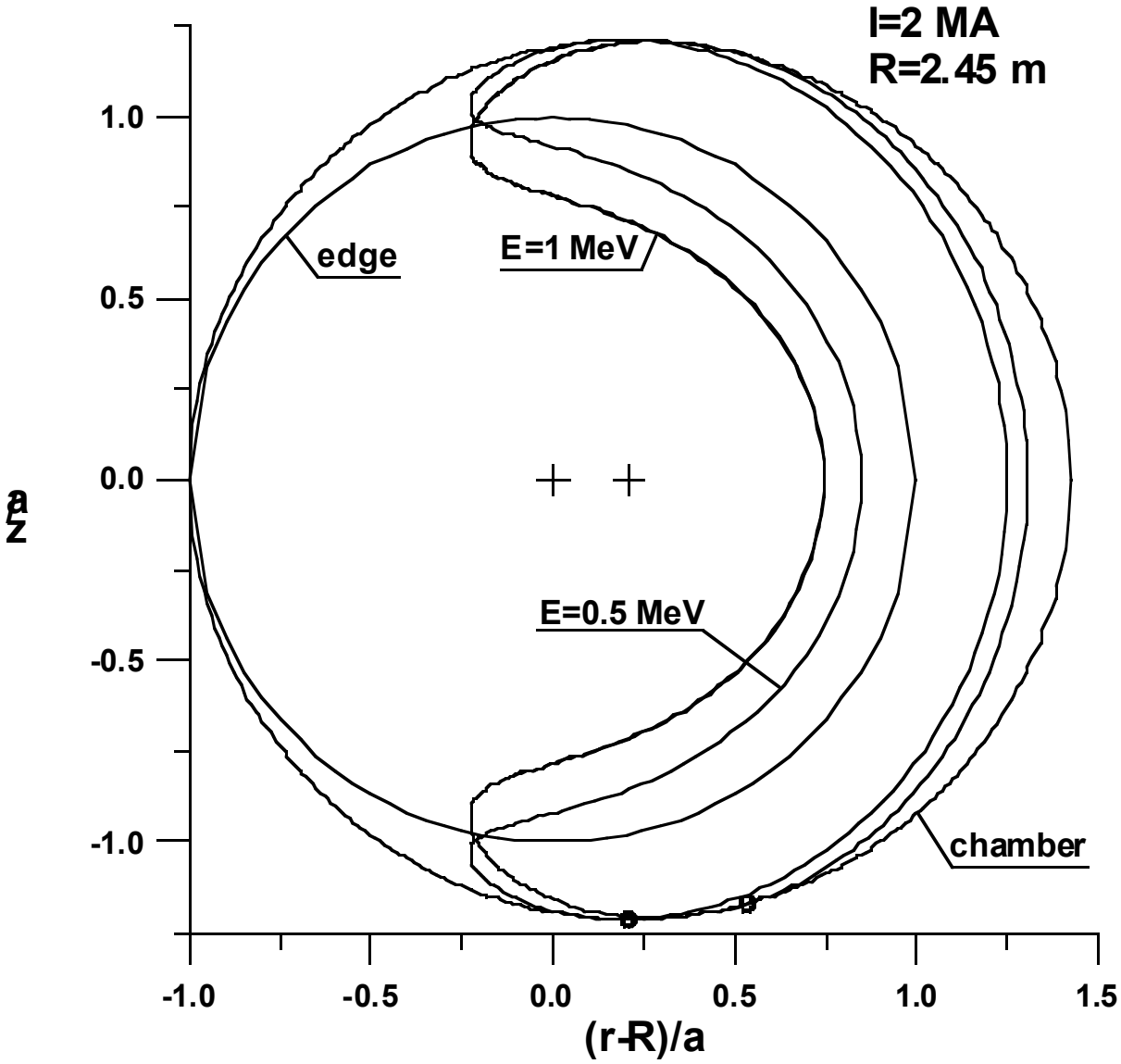
I=2 MA
R=2.45 m
edge
E=1 MeV
E=0.5 MeV
chamber
1.0
0.5
0.0
-0.5
-1.0
z/a
-1.0
-0.5
0.0
0.5
1.0
1.5
(r-R)/a

Fig. 4

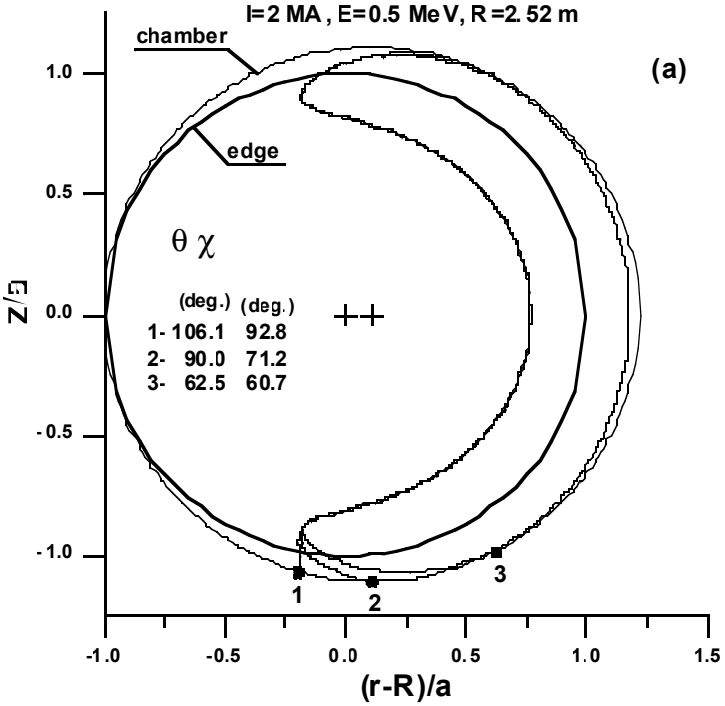
I=2 MA , E=0.5 MeV, R =2. 52 m
chamber
edge
(a)
θ χ
(deg.) (deg.)
1- 106.1 92.8
2- 90.0 71.2
3- 62.5 60.7
1
2
3
Z/a
(r-R)/a

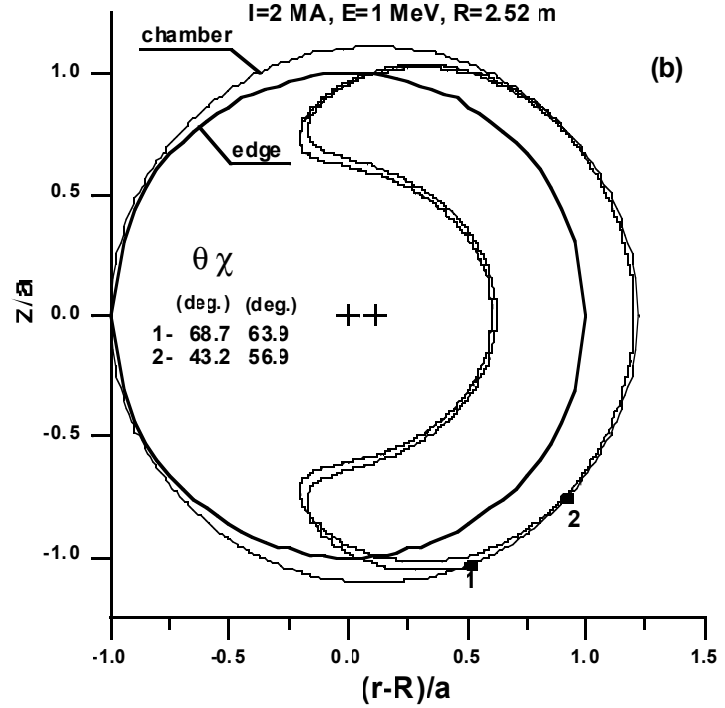
I=2 MA, E=1 MeV, R=2.52 m
chamber
edge
(b)
θ χ
(deg.) (deg.)
1- 68.7 63.9
2- 43.2 56.9
1
2
Z/a
(r-R)/a

Fig. 5

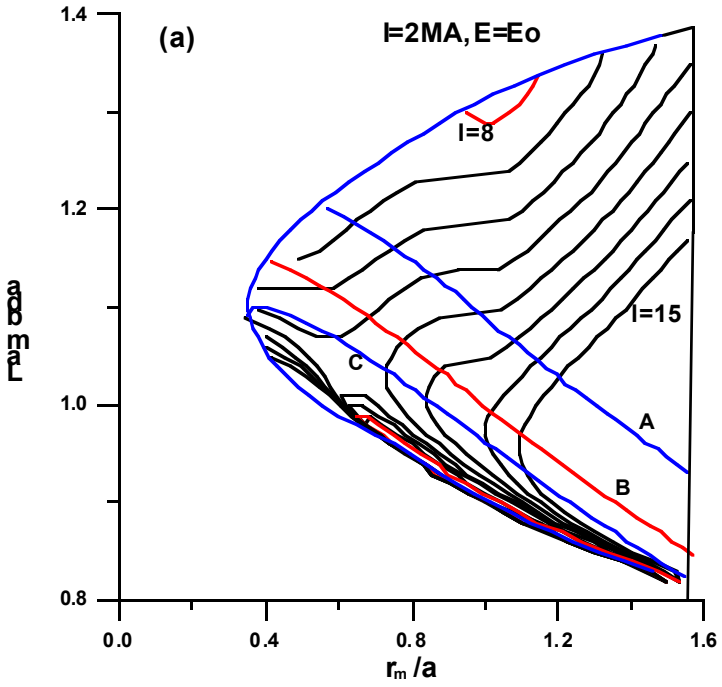
(a)
I=2MA, E=Eo
I=8
I=15
C
A
B
1.4
1.2
1.0
0.8
0.0
0.4
0.8
1.2
1.6
r_m /a

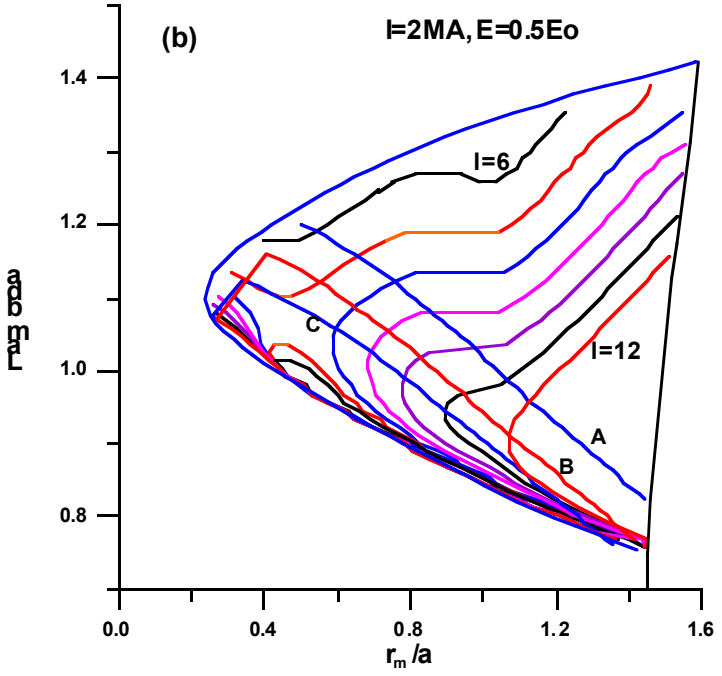
(b)
I=2MA, E=0.5Eo
I=6
I=12
C
A
B
1.4
1.2
1.0
0.8
0.0
0.4
0.8
1.2
1.6
r_m /a

Fig. 6

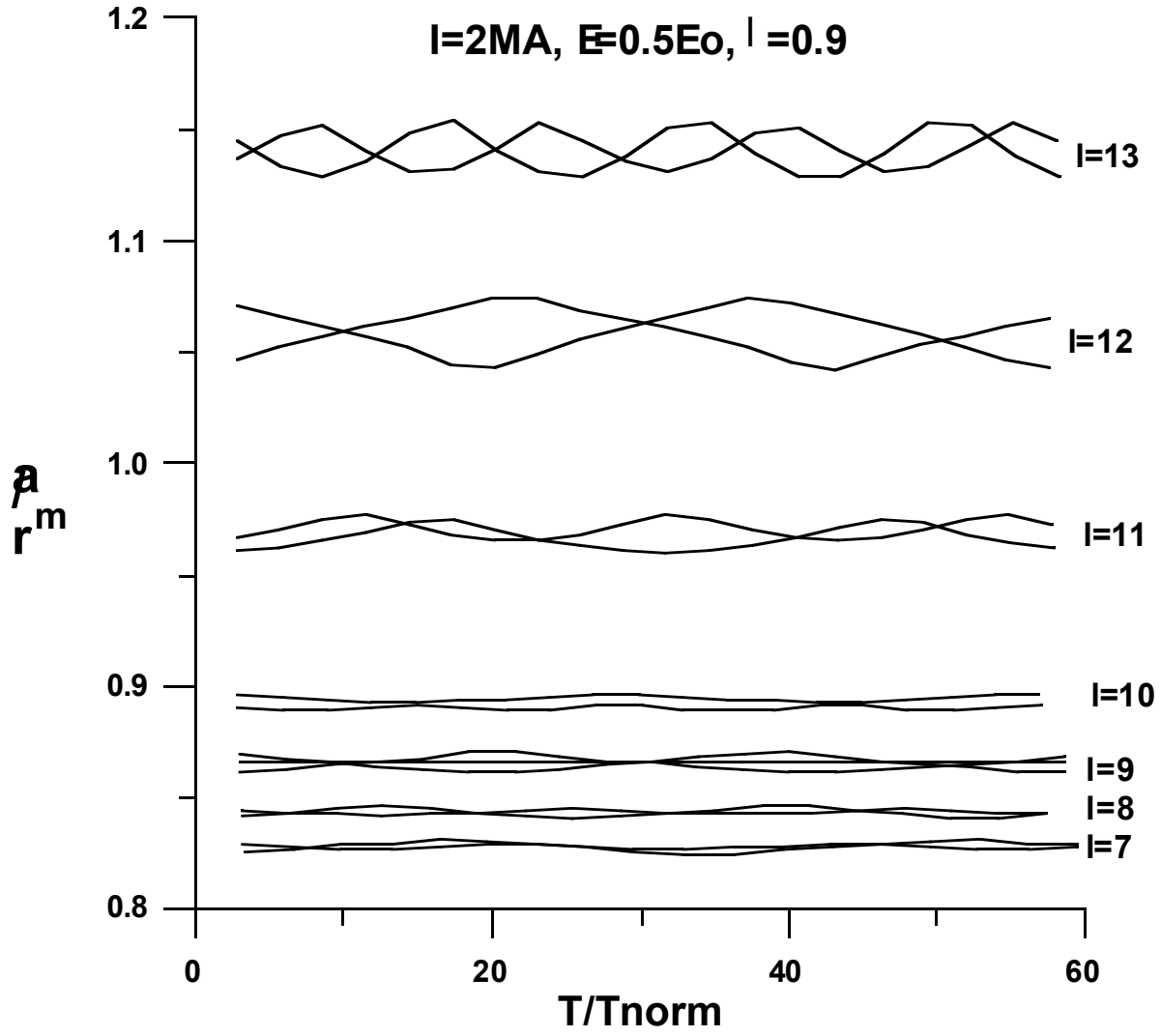
I=2MA, E=0.5Eo, | =0.9
1.2
1.1
1.0
0.9
0.8
a/r m
I=13
I=12
I=11
I=10
I=9
I=8
I=7
0
20
40
60
T/Tnorm

Fig. 7

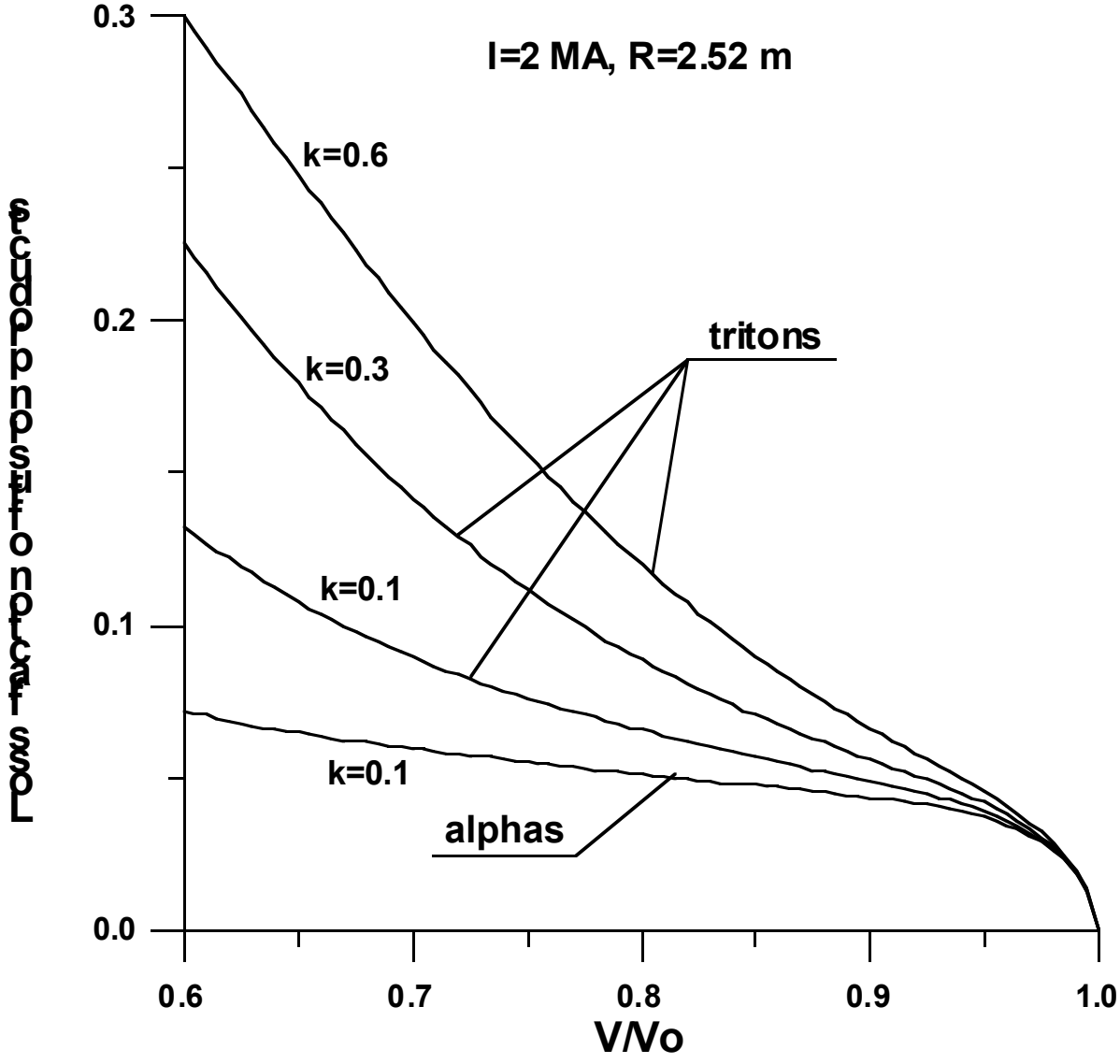
I=2 MA, R=2.52 m
k=0.6
k=0.3
k=0.1
k=0.1
tritons
alphas
0.3
0.2
0.1
0.0
0.6
0.7
0.8
0.9
1.0
V/Vo

Fig. 8

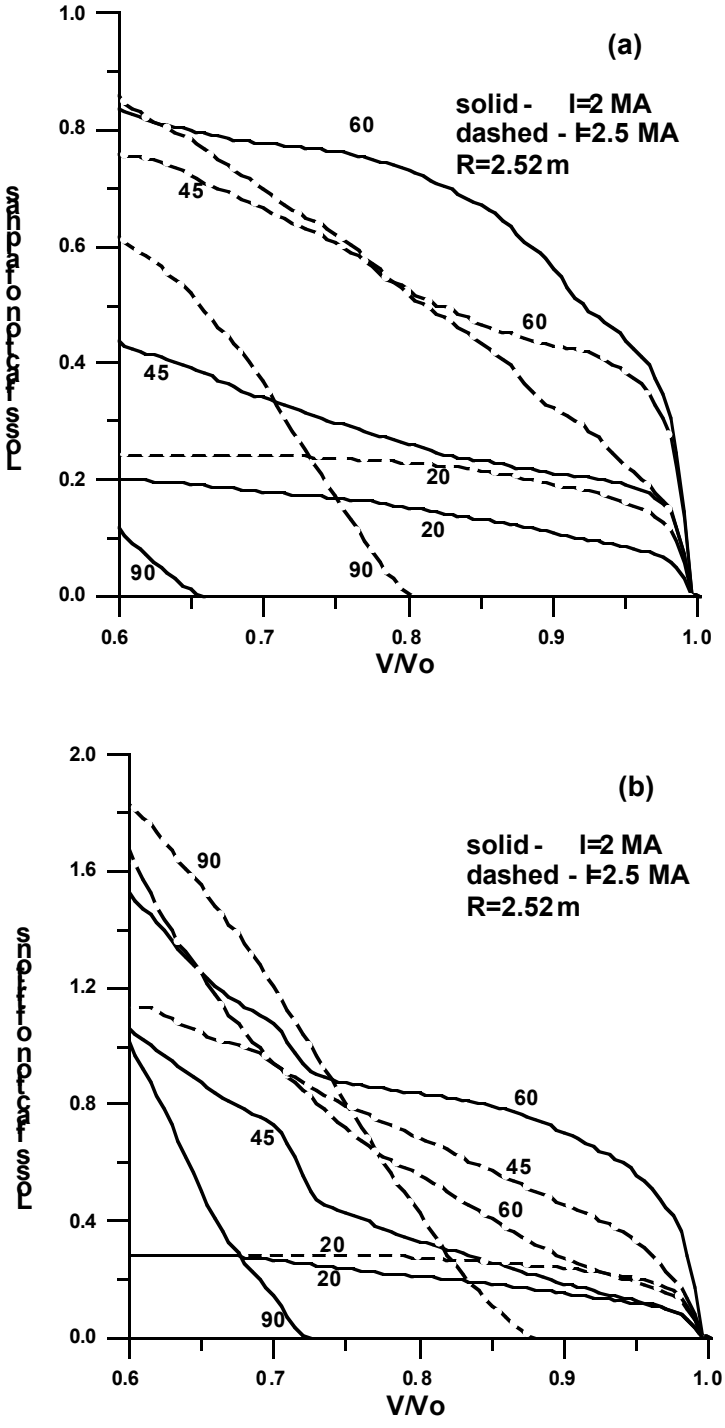
(a)
solid - I=2 MA
dashed - I=2.5 MA
R=2.52 m
60
45
60
45
20
20
90
90
1.0
0.8
0.6
0.4
0.2
0.0
0.6
0.7
0.8
0.9
1.0
V/Vo
(b)
solid - I=2 MA
dashed - I=2.5 MA
R=2.52 m
90
60
45
60
45
20
20
90
2.0
1.6
1.2
0.8
0.4
0.0
0.6
0.7
0.8
0.9
1.0
V/Vo

Fig. 9

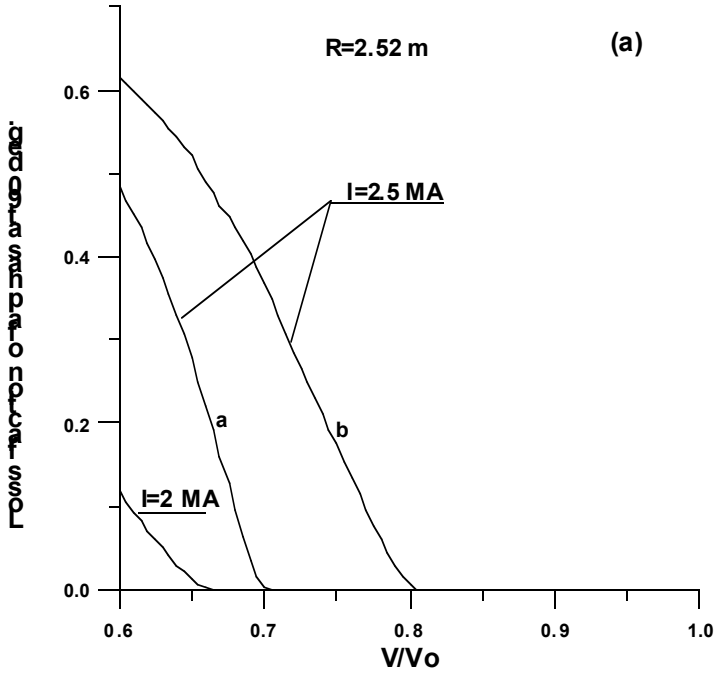
R=2.52 m
(a)
I=2.5 MA
I=2 MA
a
b
0.0
0.2
0.4
0.6
0.6
0.7
0.8
0.9
1.0
V/Vo

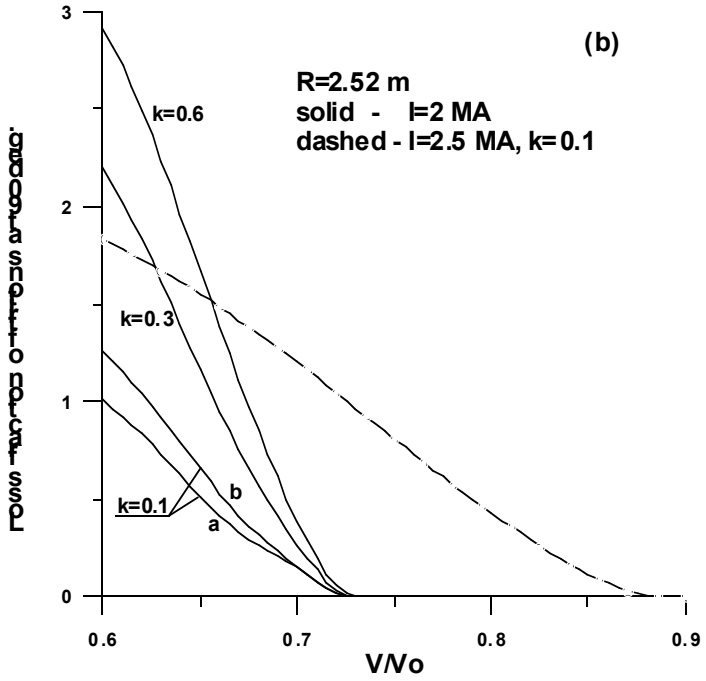
(b)
R=2.52 m
solid - I=2 MA
dashed - I=2.5 MA, k=0.1
k=0.6
k=0.3
k=0.1
a
b
0
1
2
3
0.6
0.7
0.8
0.9
V/Vo

Fig. 10

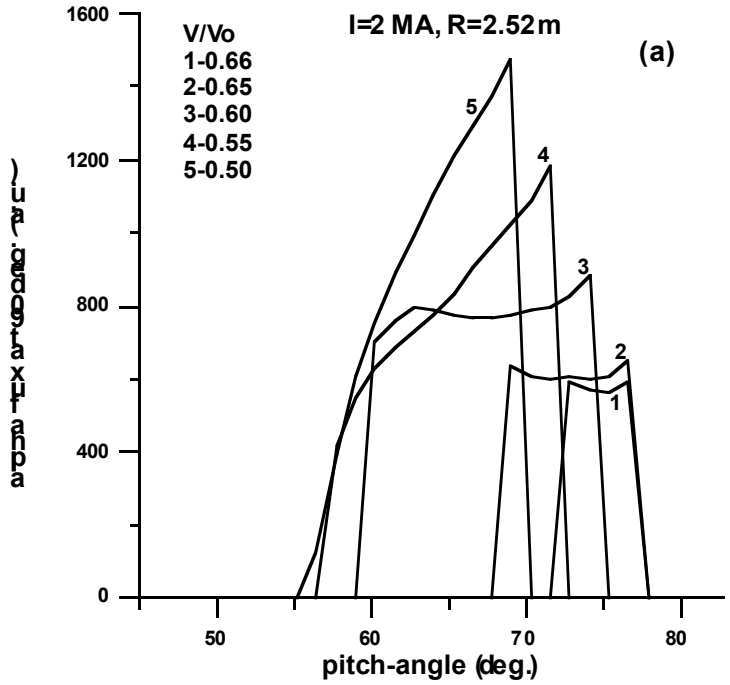
I=2 MA, R=2.52m
(a)
V/Vo
1-0.66
2-0.65
3-0.60
4-0.55
5-0.50
1600
1200
800
400
0
50
60
70
80
pitch-angle (deg.)
1
2
3
4
5

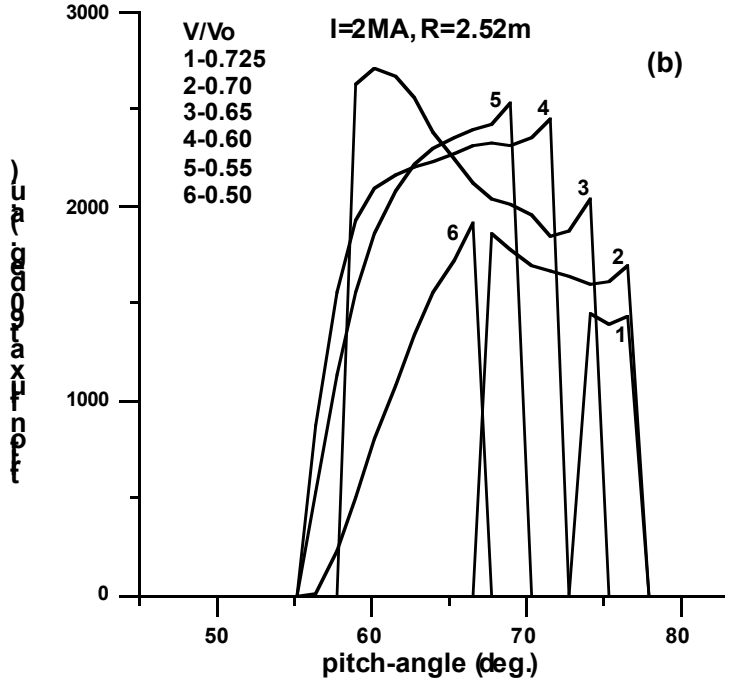
I=2MA, R=2.52m
(b)
V/Vo
1-0.725
2-0.70
3-0.65
4-0.60
5-0.55
6-0.50
3000
2000
1000
0
50
60
70
80
pitch-angle (deg.)
1
2
3
4
5
6

Fig. 11